



Controlled preparation and highly photocatalytic activity of portable MCC-g-GMA@TiO₂ photocatalyst by pre-radiation grafting-embedding method



Yue-Sheng Li ^{a,*},¹ Jiang-Tao Qin ^{b,1}, Yan Han ^c, Ji-Fu Du ^a, Zhi-Bing Dong ^d, Shao-Fa Sun ^a, Yi Liu ^{c,e,*}

^a Non-power Nuclear Technology Collaborative Innovation Center, Hubei University of Science & Technology, Hubei, Xianning 437100, PR China

^b The Education Ministry Key Lab of Resource Chemistry, Shanghai Normal University, Shanghai 200234, PR China

^c State Key Laboratory of Virology & Key Laboratory of Analytical Chemistry for Biology and Medicine (MOE), College of Chemistry and Molecular Sciences, Wuhan University, Wuhan 430072, PR China

^d School of Chemistry and Environmental Engineering, Wuhan Institute of Technology, Wuhan 430074, PR China

^e College of Chemistry and Chemical Engineering, Wuhan University of Science and Technology, Wuhan 430081, PR China

ARTICLE INFO

Article history:

Received 5 January 2017
Received in revised form 2 March 2017
Accepted 29 March 2017
Available online 16 June 2017

Keywords:

MCC
TiO₂
Grafting-embedding
Electron beam radiation
Portable photocatalyst

ABSTRACT

A portable and high efficient photocatalytic properties of MCC-g-GMA@TiO₂ (MGT) photocatalyst based on micocrystalline cellulose (MCC) surfaces is prepared by pre-radiation grafting-embedding method. TiO₂ nanoparticles were successfully introduced into the surfaces of novel MCC resin and manifested by FTIR, TG, XRD. Microstructure of MGT was characterized further by FESEM-EDS, FESEM-EDX mapping, HRTEM and BET. The highly photocatalytic activity of MGT was tested by the degradation of methyl blue dye (MB) in the aqueous medium under Xenon arc lamp. The results showed that the portable MGT resin complex system also had a highest photocatalytic performance at the appropriate content of TiO₂ (4.22 wt%) and suitable radiation dose (60 kGy). Perhaps primary reasons were attributed to the synergistic effect of adsorption-enrichment and photocatalytic degradation. In addition, the high recycling ability of MGT complex confirms that photocatalyst is highly photostability and exhibited good separation-free. Overall, this portable MGT photocatalyst has good potential for application in the field of water pollution treatment.

© 2017 Elsevier B.V. All rights reserved.

1. Introduction

Nano-TiO₂ materials are expected to play an important role in the field of environmental pollution due to its good characteristics of nontoxicity, light stability, chemical stability, powerful oxidation, low cost and totally removal of pollutants [1,2]. Recently, a lot of novel highly photocatalytic activity of TiO₂ photocatalysts based on the change of lattices or surface structures have been prepared by different methods, such as doped, coated, sensitized, composited, surface modified and so on [3,4]. However, it is still difficult to separate photocatalyst nanoparticles from reacted solutions, and this may cause secondary pollution to the environment [5]. To solve this problem, appropriate modification of photocatalyst nanoparticles with renewable porous carrier such as hydrogel

[6–9], composite resin [10,11], aerogel [12–14], xerogel [15] have been very impressive. Therefore, it is particularly important to choose the right means of modification and make sure more porous and active sites of photocatalysts as much as possible exposure to the surface of carriers.

Microcrystalline cellulose (MCC) is one of the most abundant natural renewable materials, has been received great attention as carrier matrix, in terms of its hydrophilicity, biocompatibility and abundance in nature. As highly crystalline structure consisting of repeated units of glucose linked via-1,4 glycosidic bonds so as to generate easily free radicals and trigger other reactions [16]. Some novel photocatalysts have been synthesized based on cellulose matrix by common chemical methods and exhibited good photocatalytic activities [17–19]. However, most of the photocatalysts were encased internally in cellulose and reduced the catalytic activity and efficiency of adsorption, also amplified the regenerate difficulty. Pre-radiation grafting-embedding is a simple and versatile method of embedding nanoparticles into the surface of porous carrier, radiation induced processes have a number of distinctive advantages comparing with conventional chemical methods, such

* Corresponding authors.

E-mail addresses: frank78929@163.com (Y.-S. Li), [\(Y. Liu\).](mailto:yiliuchem@whu.edu.cn)

¹ Co-first authors.

as high efficiency, free of initiator, no trick control of experimental conditions required and without limitation in trunk polymer shape [20–23]. Recently, radiation method has been widely used to immobilize inorganic semiconductor catalysts into natural polymer matrix for degradation of dyes [24–27] or antimicrobial [28–30]. A lot of inspiration were obtained from above these reports, so nano-TiO₂ may be introduced efficiently into the surface of MCC when some monomer was grafted onto MCC by electron beam radiation grafting method, which can make TiO₂ absorb effectively light energy and improve the adsorption performance, what's more, the stability, mechanical and recycling properties of composite photocatalyst system were improved subsequently. However, little detailed study has been devoted to MGT portable photocatalyst by pre-radiation grafting-embedding.

In this paper, to determine the excellent photocatalytic properties of MGT, a series of MGT portable photocatalysts were prepared by pre-radiation grafting-embedding method at room temperature and characterized by FTIR, XRD, TG, SEM, FESEM-EDS, FESEM-EDX mapping, HRTEM, BET. The highly photocatalytic activity of MGT was tested by the degradation of MB in the aqueous medium under Xenon arc lamp. The results showed that the portable MGT resin complex system also had a highest photocatalytic performance at the appropriate content of TiO₂ (4.22 wt%) and suitable radiation dose (60 kGy). MGT is easier to recycle TiO₂ nanoparticles from solutions and avoid secondary pollution to the environment after reaction. The recycling ability of MGT composite photocatalyst has highly photo-stability and exhibited good separation-free. It is very important for MGT to treat the wastewater and other environmental pollution.

2. Experimental

2.1. Materials

TiO₂ (P25) nanoparticles, (average particle size of 30–50 nm) were from Germany Degussa. Microcrystalline cellulose microspheres (MCC) (average particle size of 200±20 μm) were purchased from Asahi Kasei Chemicals Corporation (Japan). Glycidyl methacrylate (GMA) and Tween 20 were supplied by Guoyao Reagent Co., Ltd. Methyl blue dye (MB) and other reagents were purchased from Wuhan Shengshi Optical Technology Co., Ltd. All the chemicals are analytical grade and used as purchased without further purification.

2.2. Preparation of MGT by pre-radiation grafting-embedding method

MCC (5.0g) was putted into polyethylene bag and sealed succedently in vacuum. The samples were irradiated at doses of 20–100 kGy and at a dose rate of 10 kGy/pass under the cool-

ing of dry-ice by a 1 MeV electron accelerator (Wasik Associates, USA). After getting rid of oxygen with nitrogen flow, 50.0 g emulsion solution (GMA, Tween 20 and TiO₂) was injected into the three flasks. Then, the pre-radiated of MCC was added into above the emulsion solution, and continued to inlet with nitrogen. The grafting-embedding reaction was then performed in a water bath at 50 °C for 2 h. The homo-polymer, unreacted monomer and the TiO₂ which are not embedded in the MGT were removed by washing with acetone and a large amount of deionized water in the stainless steel metal screen with 200 meshes, and then the MGT were dried in vacuum at 80 °C for 24 h. The as-received samples were denoted as MGTX, where X corresponded to different concentration of GMA.

2.3. Theoretical calculation

The grafting yield (GY) was calculated using Eq. (1)

$$GY(\%) = \frac{W_g - W_0}{W_0} \times 100 \quad (1)$$

Where W_0 and W_g were the weights of MCC, MGT respectively

The embedding yield (EY) was calculated using Eq. (2):

$$EY(\%) = \frac{W_t}{W_i} \times 100 \quad (2)$$

Where W_i and W_t were the weights of the TiO₂ initial inventory and embedded of TiO₂.

2.4. Characterization

Fourier transform infrared spectra (FTIR) were recorded on a Nicolet IS10 spectrometer (Thermo Fisher Nicolet, America) in the range of 4000–400 cm⁻¹. The crystal structures of the products were characterized by X-ray powder diffraction (DMAX-D8X, Rigaku, Japan). The patterns with Cu-Kα radiation ($\lambda=0.15406$ nm) at 20 keV and 10 mA were recorded in the 2θ range of 10°–80° (2θ) with the scan speed of 4° min⁻¹. The content and component of TiO₂ in composites was determined by thermo gravimetric analysis (TG209 F3, NETZSC, German) at a heating rate of 10°Cmin⁻¹ from 30 to 800 °C in air[31]. The morphology and microstructure were characterized by a field emission scanning electron microscope (FE-SEM, ZEISS Merlin Compact VP, Germany), energy dispersive X-ray spectroscopy (Oxford Instruments Link ISIS) and HRTEM (JEOL, JSM-2010), surface element analysis was conducted using FESEM-EDS (Quanta 200, FEI, Netherlands). Nitrogen adsorption/desorption isotherms were collected on a Quantachrome NOVA-Touch surface area and porosity analyzer at 77 K after the sample had been degassed in the flow of N₂ at 120 °C for 5 h. The Brunauer-Emmett-Teller (BET) surface area was calculated from the linear part of the BET plot (P/P_0 , 0.1 – 0.25).

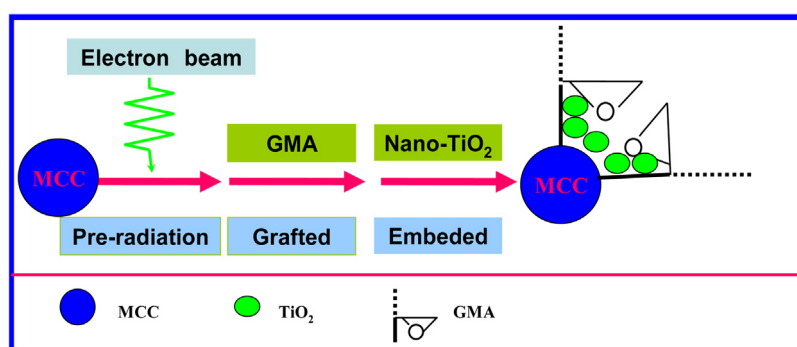


Fig. 1. Schemes of the synthetic process of the MGT composite resin.

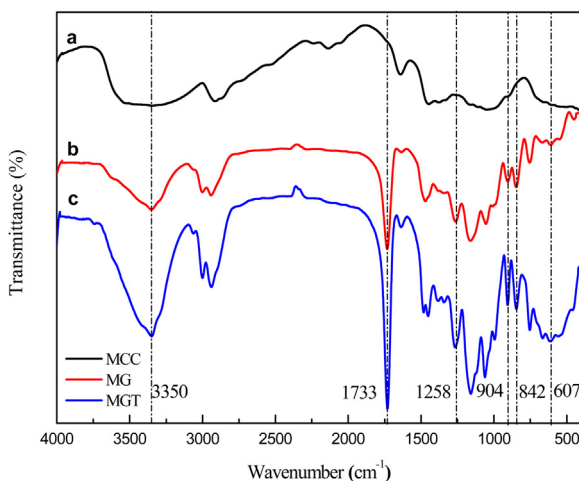


Fig. 2. FTIR spectra of MCC(a), MG(b) and MGT20(c).

2.5. Measurement of photocatalytic activity of MGT

The photocatalytic activities of MGT were tested by using MB solution. 100 mg photocatalyst was immersed into MB solution (100 mL, 4 mg/L) for 1.0 h in the dark to ensure the adsorption-desorption equilibrium. Then the MB solution including the sample was illuminated under a 500 W Xenon arc lamp at 12 cm away from the solution. The change of MB concentration was monitored by UV-vis spectrophotometer at a wavelength of 664 nm. After each typical photocatalytic experiment, recycling experiments were executed by filtering with stainless steel metal screen with 200 meshes, washing with acetone and water. The recycled products were used as catalysts to remove MB from water. Reusability of the MGT composite was investigated by repeating the experiment for five times. The concentrations of MB (4 mg/L) and inventors of catalyst (1 g/L) were maintained throughout the process of analysis.

The Langmuir-Hinshelwood model Eq. (3) was used to determine the photodegradation rate of used dyes[32].

$$\ln(c_0/c_t) = kt \quad (3)$$

Where k is the pseudo-first-order rate constant, c_0 and c_t denote the initial and final concentrations, and t represents the degradation time.

3. Results and discussion

3.1. Structural study

Preparation of MCC-g-GMA@TiO₂ by electron beam pre-radiation grafting –embedding method is shown in Fig. 1. In process of the electron beam radiation, the surface of the MCC decomposes firstly to form a mass of trapped radicals[33], then monomer were grafted onto the surface of MCC by trapped radicals in the presence of high vacuum or inert gas later. At the same time, TiO₂ nanoparticles were embedded and located onto the surface of the MCC.

FT-IR spectra of MCC, MCC-g-GMA and MCC-g-GMA@TiO₂ are shown in Fig. 2. In the spectra of MCC, the intensive and broad band at 3200–3550 cm⁻¹ are ascribed to the stretching vibrations of –OH and 1450 cm⁻¹ were assigned to the CH–OH bending vibrations. After GMA was Grafted onto MCC, which was confirmed by the new peaks presented at 842 cm⁻¹, 904 cm⁻¹ and 1258 cm⁻¹, corresponding to the characteristic peaks of epoxy groups[24,34]. Furthermore, sharp bands at 1730 cm⁻¹ assigning to carbonyl group (C=O) of GMA. After radiation grafting-embedding reaction, the successful introduction of TiO₂ was confirmed by the presence of intensive and broad absorption bands at 607 cm⁻¹, which was assigned to the stretching of Ti–O–Ti vibrations. This new generation of chemical bonds and the retention of original functional groups could be useful for MGT to retain a high photocatalytic activity.

The X-ray diffraction (XRD) patterns of TiO₂, MCC, MG and MGT are shown in Fig. 3. MCC showed narrow bands at a 2θ of 22.5° and 34.6°, this demonstrated its crystalline structure, which is conducive to the formation of trapped radicals when MCC exposure in

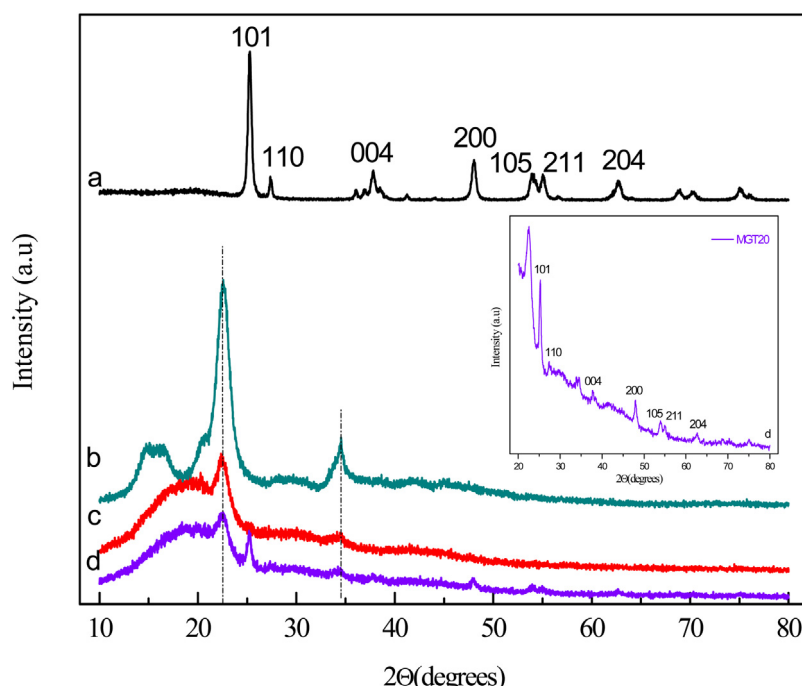


Fig. 3. XRD patterns of TiO₂(a), MCC(b), MG(c) and MGT20(d).

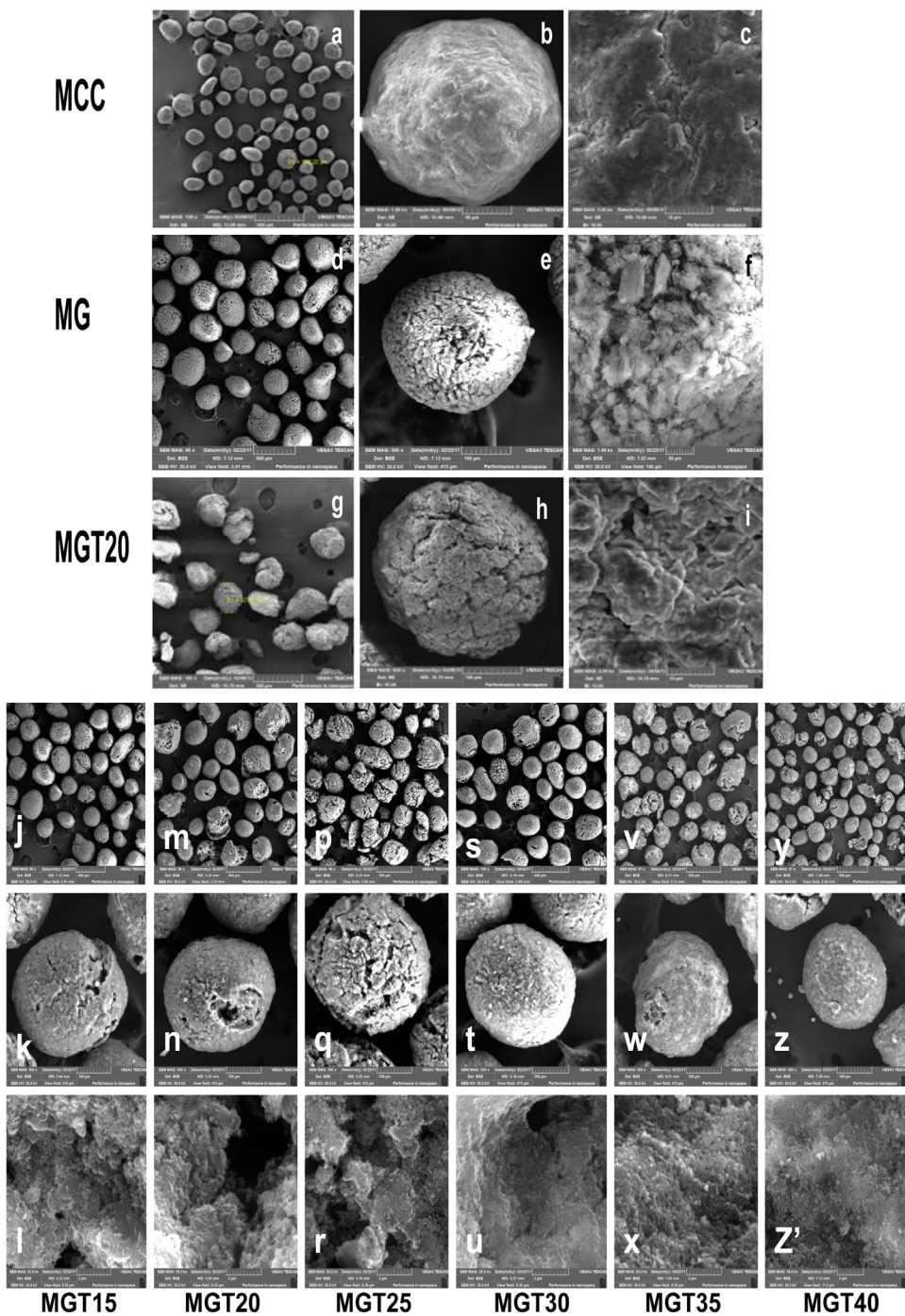


Fig. 4. SEM images of MCC (a, b, c); MG(d, e, f); MGT20(g, h, i); MGT15(j, k, l); MGT20(m, n, o); MGT25(p, q, r); MGT30(s, t, u); MGT35(v, w, x); MGT40(y, z, z').

the electron beams. Moreover, a wide semi-crystalline of steamed bread peak appeared near the 15° . After Grafting of GMA onto MCC, all the original peak intensity is reduced, which show that the crystalline of MCC was damaged due to the introduction of the GMA. The XRD diffraction peaks around 2θ of 25.4° , 37.8° , 48.1° , 54.0° , 55.0° and 62.7° , which could be indexed to the characteristic peaks (101), (004), (200), (105), (211) and (204) of anatase TiO_2 , and the peak of 27.4° could be indexed to the characteristic peak (110) of rutile TiO_2 . The XRD diffraction peaks of TiO_2 did not change significantly after TiO_2 nanoparticles were embedded into the surface of the MCC, and all original peak could be found in the MGT composite resin, but crystallization of MCC has been weakened, especially semi-crystalline of steamed bread peak appeared near

the 15° . Above the results show that TiO_2 nanoparticles were introduced firmly into the complex resin system once again and ensured to have high photocatalytic activity of MGT composite resin.

3.2. Morphology

Fig. 4 shows that the micromorphology surfaces of the MCC, MG and MGT. As shown in **Fig. 4(a–c)**, the primary particles size of MCC is $200 \pm 20 \mu\text{m}$, but they were not a regular sphere. There is no visible holes and cracks, and the surface of the microsphere is very smoothly, it were confirmed through partial enlarged detail [**Fig. 4(b, c)**]. However, the surfaces of MCC-g-GMA (MG) composite resin are more rough and the diameter is bigger than MCC. While

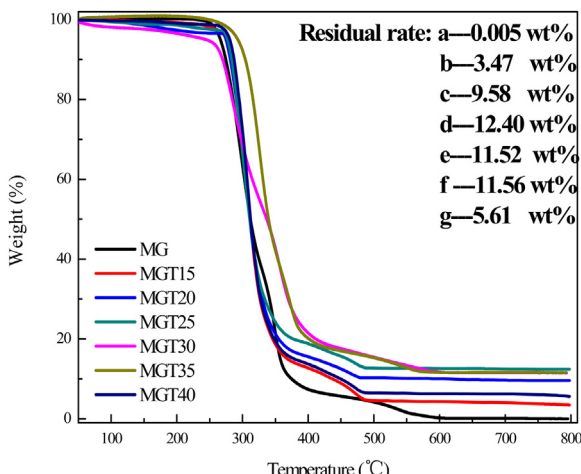


Fig. 5. Thermo gravimetric analysis profiles of different samples.

after TiO_2 nanoparticles were introduced into the MG composite resin, the microsphere diameter of MGT are increased further compared with primary MCC, and the particles size is $320 \pm 50 \mu\text{m}$ [Fig. 4(g-i)]. Because of the different embeded content of TiO_2 for MGT15 [Fig. 4(j-l)], MGT20[Fig. 4(m-o)], MGT25[Fig. 4(p-r)], MGT30[Fig. 4(s-u)], MGT35[Fig. 4(v-x)] and MGT40[Fig. 4(y, z, z')], they have the different micro-morphology surfaces and photocatalytic properties of MGTx. Moreover, the surface of MGT becomes rough owing to the nanomaterial change the surface structure of the MGT to fill the gaps and holes, the existence of the gaps and holes in the MGT resulted in a high surfaces area, and the feature maybe have great significance for its adsorption-enrichment and photocatalytic degradation.

3.3. TG analysis

The content of TiO_2 and thermal stability of complex resin were determined by thermo gravimetric analysis in air atmosphere. Fig. 5 shows the thermogram of TiO_2 -loaded and unloaded dry composite resin samples, the weight loss around 5% was slow and represented only water evaporation from room temperature to 280°C . However, the weight loss was accelerated at 280°C – 350°C , this indicated that the temperature accelerated the decomposition of grafted GMA and MCC nuclear after 280°C . Importantly, the third stage of the MGT appeared between 350°C – 500°C because of the burning of char. Compared with MGT, there was a delay phenomenon for the third stage of the MG, burning net until 600°C . Considering the above results, the thermal stability of MGT was slightly stronger than that of MG composite resin because of TiO_2 was introduced. Since the TiO_2 was relative stable, the content of TiO_2 for MGT15, MGT20, MGT25, MGT30, MGT35 and MAT40 was estimated to be about 3.47 wt%, 9.58 wt%, 12.40 wt%, 11.52 wt%, 11.56 wt% and 5.61 wt%, respectively.

3.4. FESEM-EDS and EDX mapping detection

The content of TiO_2 has been obtained by TG analysis(in Fig. 5), but the result maybe has deviation to some extend because of insufficient combustion of carbon component of MGT20 in air atmosphere. In order to prove TiO_2 was successfully introduced into the MCC surfaces by radiation grafting-embedding method and get the accurate datas, FESEM-EDS and EDX mapping technique was also used to determine precisely the microstructure, component and content of TiO_2 in Fig. 6. The morphology of MGT20 was revealed in Fig. 6(a, e, f). The elemental EDX mapping of sample clearly demonstrated the existence of Ti, O and C on MGT20 sur-

Table 1
Grafting-yield and embedding-yield of MGT.

MGT Composite Resin	GMA concentration (w/w)					
	15%	20%	25%	30%	35%	40%
Grafting yield (%)	124.9	208.1	254.4	291.3	262.7	146.3
Content of TiO_2 (%)	3.47	9.58	12.40	11.52	11.56	5.61
Embedding yield (%)	9.76	36.90	55.00	56.35	52.41	17.27

The content of TiO_2 in composites was determined by thermo gravimetric analysi; radiation dose is 60 kGy.

face (b, c, d in Fig. 6), and the distribution of these elements was quite uniform. and Fig. 6e shows that Ti, O and C elements were found on the surface of bulk MGT20, among the content of Ti is 2.46 wt%, TiO_2 content is then obtained is 4.10 wt%. Similar results were obtained for different morphologies of MGT20 in Fig. 6f, Ti, O and C elements were also found on the surface of powder MGT20, among the content of Ti is 2.53 wt%, TiO_2 content is then obtained is 4.22 wt% and more accurate than the former due to some TiO_2 nanoparticles may be infiltrated into the deeper external surfaces of MCC along the gap after radiation so as to improve a little on the content of TiO_2 . All datas are fully documented that TiO_2 was successfully introduced into the external surfaces of MCC by radiation grafting-embedding method.

3.5. HRTEM images

HRTEM is a significant characterization method for analyzing the nanostructures of nanomaterials. HRTEM images revealed that the TiO_2 particle on surfaces of MGT20 in Fig. 7, which reveals that TiO_2 are highly crystallized, as evidenced by well-defined lattice fringes(Fig. 7a-c), TiO_2 nanoparticles with sizes of 20–50 nanometers were determined, consistent with the particle sizes of TiO_2 (P25 raw material) and the FE-SEM observation(Fig. 4). The interplanar spacing of TiO_2 is 0.248 nm, corresponding to the rutile (101) plane, the interplanar spacing of TiO_2 is 0.353 nm, corresponding to the anatase (101) plane, which is in good accordance with the results of the XRD patterns shown in Fig. 3. The HRTEM analysis further confirms the existence of TiO_2 nanoparticles in the resulting samples, which provide the possibility to enhance the photocatalytic performance of MGT20.

3.6. Effect of radiation dose

The radiation dose effect of the MGT on the property of photodegradation with MB was investigated. Fig. 8 shows the degradation efficiency of MB with MGT at different radiation dose and at different time. The curves of degradation with these MGT were approximately similar, but the degradation rate is different, and the degradation efficiency depending on the radiation dose. However, it did not present regular changes. The degradation efficiency is not the best when absorbed high or low radiation dose, the high grafting-yield resulted in the embedding too deep of TiO_2 (active site was covered) when absorbed high radiation dose, but the low grafting –yield resulted in the embedding yield too few of TiO_2 when absorbed low radiation dose. Therefore only suitable radiation dose can ensure the relative higher embedding –yield, and TiO_2 nanoparticles were located into the surface of the MCC. In view of the above results, the MGT portable photocatalysts show excellent performance in the photocatalytic degradation of MB when radiation dose is 60 kGy.

3.7. Photocatalytic performances of MGT

The degradation efficiency of MB dye has been changed at different GMA concentration are shown in Fig. 9(a) and Table 1, and the

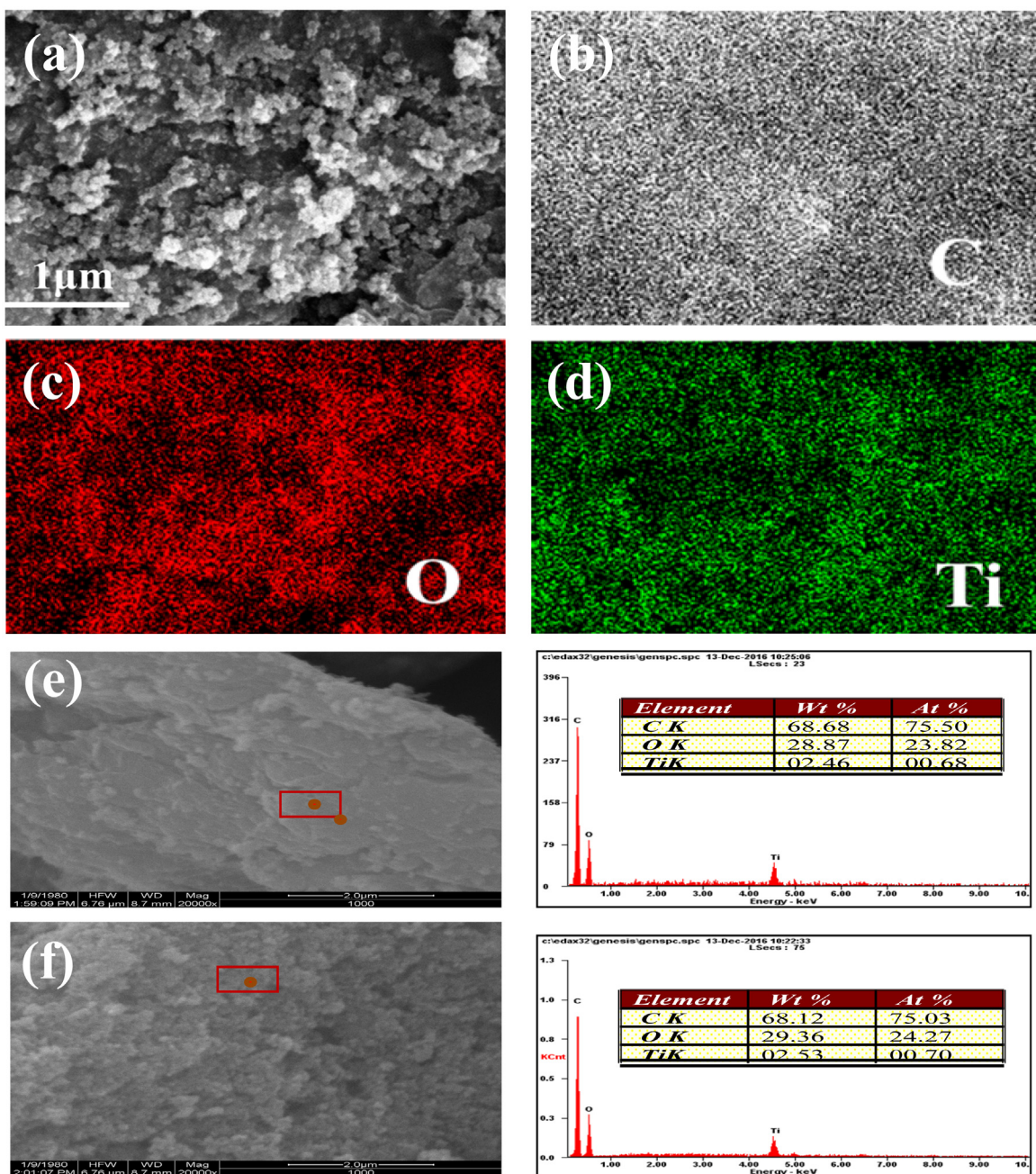


Fig. 6. FESEM-EDS (a, e, f) images and EDX mapping of major elements of MGT20 (b: C; c: O; d: Ti).

MGT degradation kinetic fitting curves are presented in Fig. 9(b). It could be concluded that the photocatalytic activity of MGT20 is slightly better than other photocatalysts, which the degradation rate was 94.6% and apparent degradation rate was $2.433 \times 10^{-2} \text{ min}^{-1}$ (in Table 2). It is well known that, the grafting ratio is related to the concentration of the monomer, which can be seen from Table 1. The degradation efficiency is not the best when the GMA concentration is high or low, because the content of TiO_2 is not very high. When the GMA concentration was 20% to 35%, the grafting-yield was more than 200% (in Table 1), and the embedding-yield was relative higher, but the rate of degradation efficiency is different owing to different embedding depth. When the GMA concentration was 25%, 30% and 35%, which the degradation rate constant were 74.3%, 83.2% and 70.2%, respectively. Although the content of

Table 2
Kinetic parameters on photocatalytic degradation of MB with different samples.

Sample	$k_{\text{app}} \times 10^{-2} (\text{min}^{-1})$	^a R	Degradation Rate (%)
MGT15	1.448	0.9894	81.2
MGT20	2.433	0.9890	94.7
MGT25	1.156	0.9800	74.3
MGT30	1.462	0.9809	83.2
MGT35	1.016	0.9821	70.2
MGT40	1.295	0.9961	78.2

^a R is the correlation coefficient.

TiO_2 (12.40 wt%, 11.52 wt%, 11.56 wt%) is very high, but the degradation rate is not very good. This is may due to the excessive depth of the active sites.

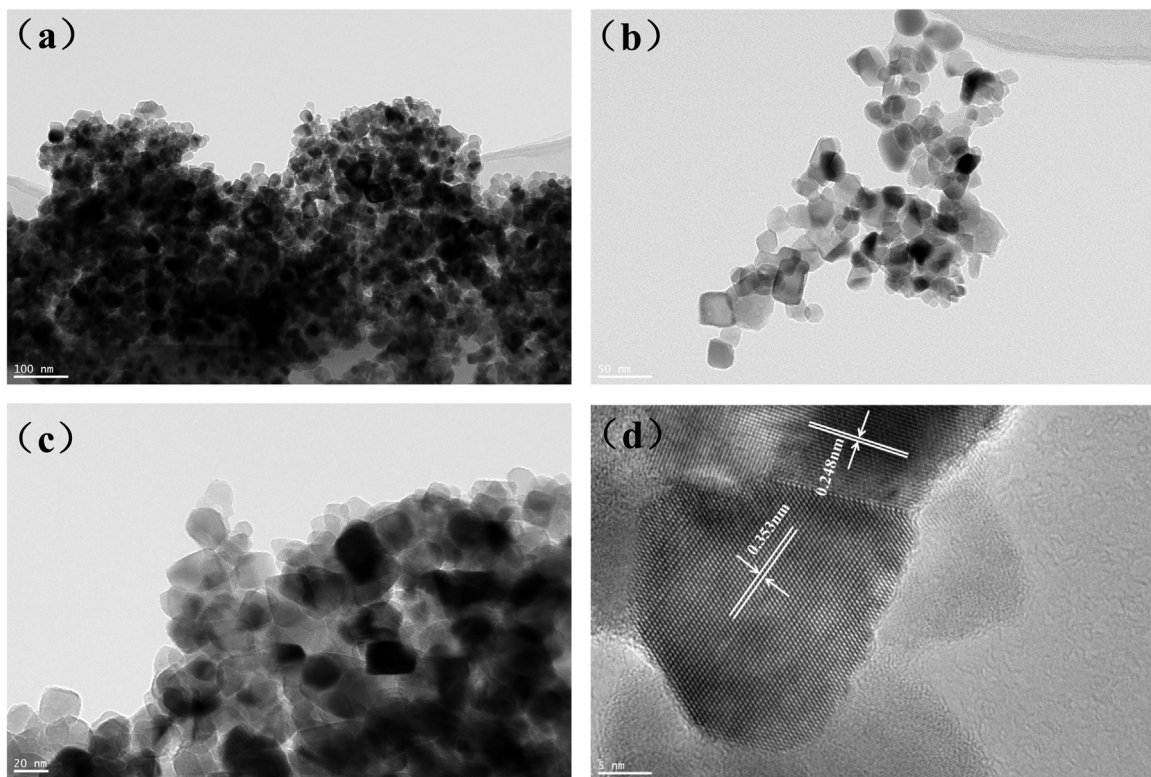


Fig. 7. HRTEM images of nano-TiO₂ on surfaces of MGT20.

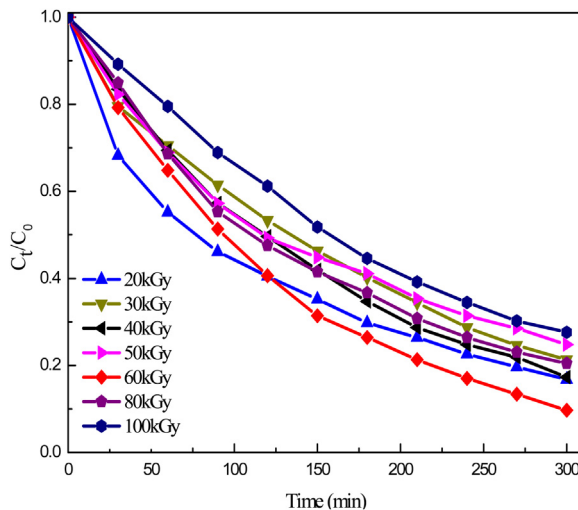


Fig. 8. Photocatalytic activities of MGT at different radiation dose.

Fig. 10 gives the cycling experiment of the photocatalytic degradation of MB in presence of MGT20. From **Fig. 10(b)**, it is clear that the degradation rate was reduced slightly from 94.6% to 85.7% after the five cycle of the degradation of MB by MGT20. Above the results, the photocatalyst is highly photostability and exhibited good separation-free owing to hierarchical structure can substantially prevent the catalyst loss and inhibit the catalyst aggregation [34].

For comparison, the photocatalytic activities of different samples [MG(a), MCC(b), MGT20(c)] were examined under xenon arc lamp light within 120 min and the results were given in **Fig. 11**.

Table 3
Physical adsorption parameters of different samples.

Sample	Surface area (m ² /g)	Pore Volume(10 ⁻³ mL/g)	Average Pore diameter(nm)
MCC	0.15	0.19	4.93
MG	1.15	4.58	7.86
MGT15	2.06	9.16	17.76
MGT20	2.41	11.04	18.33
MGT25	2.12	11.16	21.02
MGT30	1.77	6.73	15.24
MGT35	1.79	11.52	25.84
MGT40	1.26	10.82	34.44

Obviously, the MGT20 portable photocatalyst exhibits more effective photocatalytic performance for degradation of MB (94.6%) than MCC(20.5%) and MG(18.5%), which indicates that embedded TiO₂ nanoparticles were main active sites and attributed to the photocatalytic performance of MGT system, however, pure MCC and MG did not have photocatalytic activity.

3.8. Behaviors of adsorption

According to **Fig. 12(A)**, in the absence of light, about 12%–22% of MB was absorbed with different MGT samples. It could be concluded that the adsorption property of MGT20 is better than another composite resins. Which the absorbance is 20.2%, and this characteristic of high absorption can be to support MGT20 has higher photocatalytic activity. The absorption of MB with MGT20 was further confirmed by the formation of shiny and smoothly surface [**Fig. 12(B, a)**], while the smoothly surface was changed to gaps and holes after degradation [**Fig. 12(B, b)**], which is almost similar to fresh catalyst [**Fig. 4(g-i)**]. Physical adsorption parameters of different samples were also obtained by BET in **Table 3**, the results show

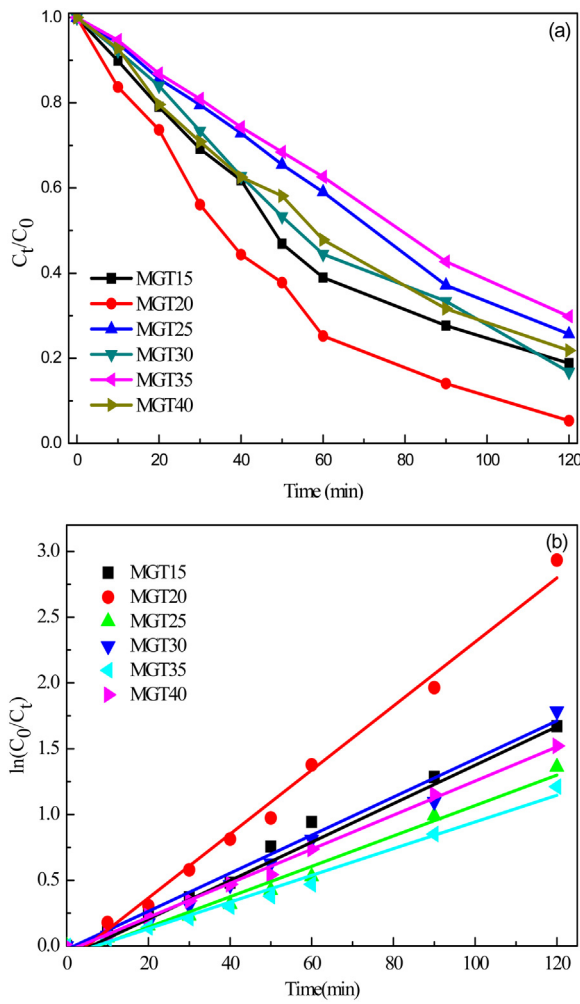


Fig. 9. (a) Photocatalytic activities of MGT at different GMA concentration. (b) Plots of $\ln(c_0/c_t)$ versus time indicating first order behavior for MGT at different GMA concentration.

that MGT20 has more higher surface area ($2.41 \text{ m}^2/\text{g}$), pore volume ($11.04 \cdot 10^{-3} \text{ mL/g}$) and average pore diameter (18.33 nm) than MCC substrate, with the change of the content of TiO_2 , different samples have different surface area, but MGT20 has the highest surface area in all the samples of determination, which is beneficial to improve the adsorption performances and all the above results were also further confirmed (Section 3.1–3.3). This portable MGT photocatalyst may be efficient for removal of organic contaminants owing to the synergistic effect of adsorption-enrichment and photocatalytic degradation synchronously [35]. It may be primary contribution to enlarge the surface area, pore volume and average pore diameter, increase adsorption quantity, short the time of adsorption and photodegradation.

3.9. Mechanism of radiation grafting-embedding and photocatalytic activity

The mechanism of radiation grafting-embedding and photocatalytic degradation on portable MGT20 photocatalyst is schemed in Figs. 1 and 13. Firstly, the surfaces of the MCC were decomposed and formed a mass of trapped radicals by electron beam pre-radiation. Secondly, GMA monomer were grafted onto the surfaces of MCC by trapped radicals in the presence of high vacuum or inert gas later. At the same time, TiO_2 nanoparticles were embedded

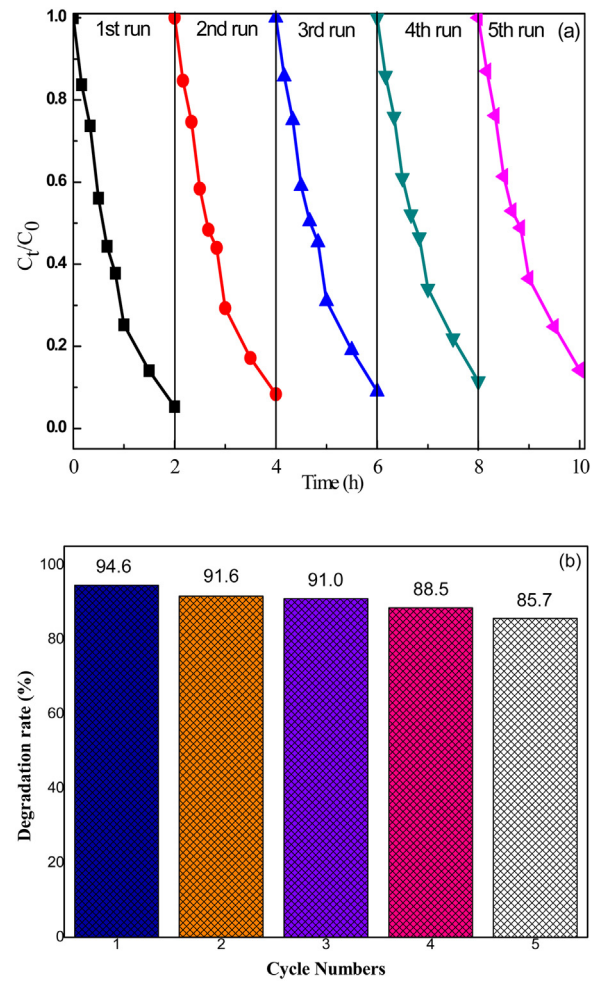


Fig. 10. (a) Cycling experiment of the photocatalytic degradation of MB in presence of MGT20 and (b) Five cycles of the degradation of MB by MGT20.

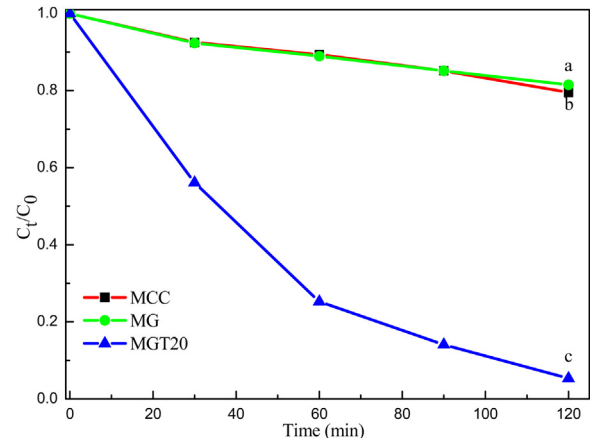


Fig. 11. Photocatalytic activities of different samples.

into the surfaces of the MCC by grafted GMA monomer. Actually, grafted-GMA monomer and embedded- TiO_2 nanoparticles were accomplished simultaneously (Fig. 1 is shown), which has been demonstrated in the above characterized results.

In Fig. 13, dye ions has played two functions: First, the dyes were absorbed into the surfaces of MGT and sensitized TiO_2 . On the

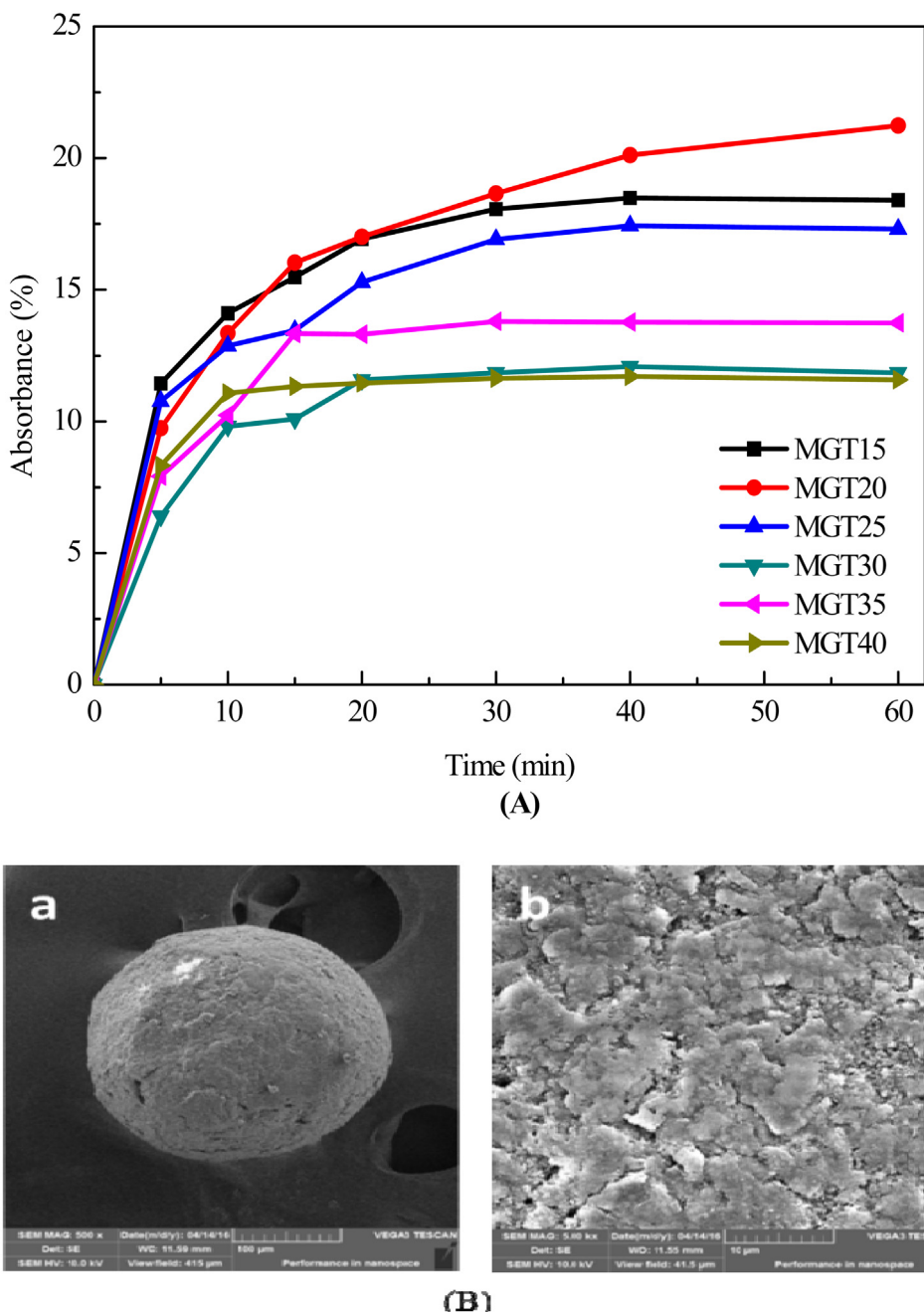


Fig. 12. (A) Adsorbance of MB with different MGT in dark and (B) SEM images of MGT20.

other hand, dye ions were decolorized by TiO_2 . The dye degradation mechanism can be expressed as follows: excitation of the adsorbed dye takes place by light to the appropriate singlet or triplet states, subsequently followed by electron ejection from the excited dye molecule onto the conduction band of the TiO_2 particles, while the dye is converted into a cationic dye radical ($\text{Dye}^{\cdot+}$) that undergoes degradation to yield product [36,37]. The dyes were removed effectively by this MGT portable photocatalyst system.

4. Conclusions

In summary, portable MCC-g-GMA@ TiO_2 (MGT) photocatalyst has been successfully prepared by pre-radiation grafting-

embedding method. TiO_2 nanoparticles were successfully introduced into the surface of novel MCC resin and manifested by FTIR, TG, XRD and FESEM-EDS. Microstructure of MGT was characterized further by SEM, FESEM, HRTEM, EDX mapping and BET. It was also found that portable photocatalysts show excellent photocatalytic degradation performance at the appropriate content of TiO_2 (4.22 wt%), suitable radiation dose (60 kGy) and the concentration of 20% w/w GMA. This portable MGT photocatalyst is efficient in removing organic contaminants owing to the synergistic effect of adsorption-enrichment and photocatalytic degradation synchronously. Also given the separation-free and photostability of MGT, it may have good potential for application in the field of water pollution treatment.

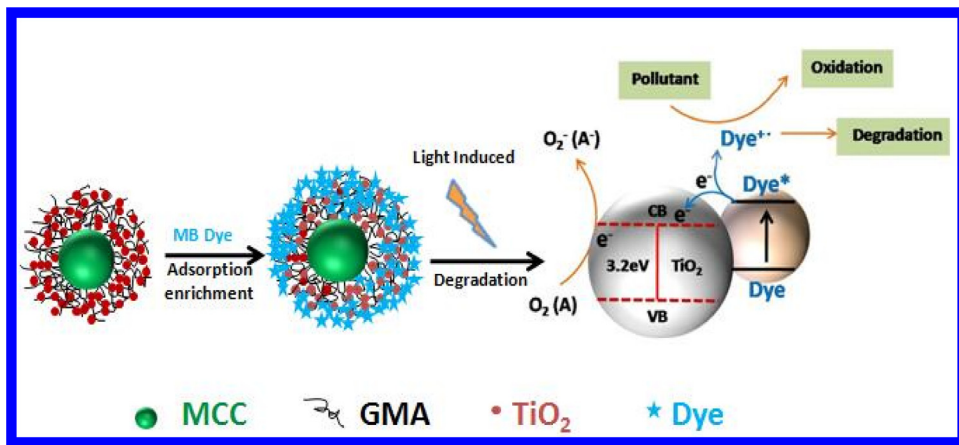


Fig. 13. Mechanism of adsorption and photocatalytic degradation on MGT20.

Acknowledgments

This work was supported by the National Natural Science Foundation of China (No. 11405050, 21302150), the National University Students Training and Entrepreneurial Practice Project (No. 201210927033, No. 20131092723), the 12th Five Year Plan of Hubei Province (No. 2014B243).

References

- [1] W. Choi, A. Termin, M.R. Hoffmann, *J. Phys. Chem. B* 98 (1994) 13669–13679.
- [2] J. Chen, C. Poon, *Build. Environ.* 44 (2009) 1899–1906.
- [3] Y.S. Li, F.L. Jiang, Q. Xiao, R. Li, K. Li, M.F. Zhang, Y. Liu, *Appl. Catal. B: Environ.* 101 (2010) 118–129.
- [4] S. Girish Kumar, K.S.R. Koteswara Rao, *Appl. Surf. Sci.* 391 (2017) 124–148.
- [5] M. Thomas, G.A. Naikoo, M.U.D. Sheikh, F.M. Bano, *J. Photochem. Photobiol. A* 327 (2016) 33–43.
- [6] W. Jiang, Y. Liu, J. Wang, M. Zhang, W. Luo, Y. Zhu, *Adv. Mater. Interface* 3 (2016), <http://dx.doi.org/10.1002/admi.201500502>.
- [7] M. Zhang, W. Jiang, D. Liu, J. Wang, Y. Zhu, Y. Liu, Y. Zhu, *Appl. Catal. B: Environ.* 183 (2016) 263–268.
- [8] A.S. Weingarten, R.V. Kazantsev, L.C. Palmer, M. McClendon, A.R. Koltonow, A.P. Samuel, S.I. Stupp, *Nat. Chem.* 6 (2014) 964–970.
- [9] D. Wu, M. Yi, H. Duan, J. Xu, Q. Wang, *Carbon* 108 (2016) 394–403.
- [10] J. Sun, S.S. Watson, D.A. Allsopp, D. Stanley, D. Skrtic, *Dent. Mater.* 32 (2016) 363–372.
- [11] R.Z. Xie, X.Y. Meng, P.Z. Sun, J.F. Niu, W.J. Jiang, L. Bottomley, D. Li, Y.S. Chen, J. Crittenden, *Appl. Catal. B Environ.* 203 (2017) 515–525.
- [12] W. Liu, J. Cai, Z. Li, *ACS Sustain. Chem. Eng.* 3 (2015) 277–282.
- [13] Z. Liu, P. Wu, S. Yang, H. Wang, C. Jin, *Int. J. Polym. Sci.* (2016), <http://dx.doi.org/10.1155/2016/9351725>.
- [14] M. Nawaz, W. Miran, J. Jang, D.S. Lee, *Appl. Catal. B: Environ.* 203 (2017) 85–95.
- [15] B.G. Esther, A. Elmouwahidi, M.A. Álvarez, C.M. Francisco, F.P.C. Agustín, J.M.H. Francisco, *Appl. Catal. B: Environ.* 201 (2017) 29–40.
- [16] J. Hao, S.Y. Xu, N.Y. Xu, D.X. Li, R.J. Linhardt, Z.Q. Zhang, *Carbohydr. Polym.* 155 (2017) 483–490.
- [17] Q. Wang, J. Cai, L. Zhang, *Cellulose* 21 (2014) 3371–3382.
- [18] K. Tu, Q. Wang, A. Lu, L. Zhang, *J. Phys. Chem. C* 118 (2014) 7202–7210.
- [19] Y. Jiao, C. Wan, J. Li, *Appl. Phys. A* 120 (2015) 341–347.
- [20] Z. Dong, J. Zhao, J. Du, C. Li, L. Zhao, *Radiat. Phys. Chem.* 126 (2016) 68–74.
- [21] L. Zhao, J. Sun, Y. Zhao, L. Xu, M.L. Zhai, *Chem. Eng. J.* 170 (2011) 162–169.
- [22] J. Wu, M.D. Soucek, *Radiat. Phys. Chem.* 119 (2016) 55–63.
- [23] B.I. Kharisov, O.V. Kharissova, U.O. Méndez, *Radiation Synthesis of Materials and Compounds*, CRC Press, 2016.
- [24] A.A. Essawy, A.E.H. Ali, M.S.A. Abdel-Mottaleb, *J. Hazard. Mater.* 157 (2008) 547–552.
- [25] M.M. Sari, *Water Sci. Technol.* 61 (2010) 2097–2104.
- [26] A.E.H. Ali, A.I. Raafat, G.A. Mahmoud, N.A. Badway, M.A. El-Mottaleb, M.F. Elshahawy, *J. Inorg. Organomet. Polym. Mater.* 26 (2016) 606–615.
- [27] F.W. Wu, W. Liu, J.L. Qiu, J.Z. Li, W.Y. Zhou, Y.P. Fang, S.T. Zhang, X. Li, *Appl. Surf. Sci.* 358 (2015) 425–435.
- [28] M.R. Khafaga, H.E. Ali, A.W.M. El-Naggar, *J. Text. Inst.* 107 (2016) 766–773.
- [29] K. Hareesh, A.V. Deore, S.S. Dahiwale, G. Sanjeev, D. Kanjilal, S. Ojha, S.D. Dhole, *Radiat. Phys. Chem.* 112 (2015) 97–103.
- [30] Y.S. Li, Y. Han, J.T. Qin, Z.Y. Song, H.H. Cai, J.F. Du, Y. Liu, *J. Appl. Polym. Sci.* 133 (2016) 44150.
- [31] X. Jiang, X. Zhu, X. Liu, L. Xiao, X. Ai, H. Yang, Cao, Y. Cao, *Electrochim. Acta* 196 (2016) 431–439.
- [32] T. Bhowmik, M.K. Kundu, S. Barman, *RSC Adv.* 5 (2015) 38760–38773.
- [33] A. Alberti, S. Bertini, G. Gastaldi, N. Iannaccone, D. Macciantelli, G. Torri, E. Vismara, *Eur. Polym. J.* 41 (2005) 1787–1797.
- [34] J. Miao, A. Xie, S. Li, F. Huang, J. Cao, Y. Shen, *Appl. Surf. Sci.* 360 (2016) 594–600.
- [35] W. Jiang, W. Luo, R. Zong, W. Yao, Z. Li, Y. Zhu, *Small* 12 (2016) 4370–4378.
- [36] F. Zhang, J. Zhao, T. Shen, *Appl. Catal. B: Environ.* 15 (1998) 147–156.
- [37] J.S. Im, B.C. Bai, S.J. In, *J. Colloid Interface Sci.* 346 (2010) 216–221.